https://doi.org/10.1063/9.0000554

Cite:
M. L. Arreguín-Hernández, A. Dzubinska, M. Reiffers, J. L. Sánchez Llamazares, C. F. Sánchez-Valdés, R. Varga; Magnetostructural transition and magnetocaloric effect in Mn0.5Fe0.5NiSi1−xAlx melt-spun ribbons (x = 0.055 and 0.060). AIP Advances 1 February 2023; 13 (2): 025336. https://doi.org/10.1063/9.0000554

RESEARCH ARTICLE | FEBRUARY 08 2023

Magnetostructural transition and magnetocaloric effect in $Mn_{0.5}Fe_{0.5}NiSi_{1-x}Al_x$ melt-spun ribbons (x = 0.055 and 0.060)

Special Collection: 67th Annual Conference on Magnetism and Magnetic Materials

M. L. Arreguín-Hernández ; A. Dzubinska ; M. Reiffers ; J. L. Sánchez Llamazares ; C. F. Sánchez-Valdés ; R. Varga

AIP Advances 13, 025336 (2023)
https://doi.org/10.1063/9.0000554

Magnetostructural transition and magnetocaloric effect in $Mn_{0.5}Fe_{0.5}NiSi_{1-x}Al_x$ melt-spun ribbons (x = 0.055 and 0.060)

Cite as: AIP Advances 13, 025336 (2023); doi: 10.1063/9.0000554
Submitted: 3 October 2022 • Accepted: 5 December 2022 •
Published Online: 8 February 2023

M. L. Arreguín-Hernández,[1,2,a] A. Dzubinska,[2] M. Reiffers,[3] J. L. Sánchez Llamazares,[1,4,a] C. F. Sánchez-Valdés,[5] and R. Varga[2]

AFFILIATIONS

[1] Instituto Potosino de Investigación Científica y Tecnológica A.C., Camino a la Presa de San José 2055, Col. Lomas 4a, San Luis Potosí S.L.P. 78216, Mexico
[2] CPM-TIP, UPJS, 041 01 Kosice, Slovakia
[3] Faculty of Humanities and Natural Sciences, University of Presov, Ul. 17. Novembra1, 080 01 Presov, Slovakia
[4] Departamento de Fisica, Universidad de Oviedo, 33007 Oviedo, Spain
[5] Departamento de Física y Matemáticas, División Multidisciplinaria en Ciudad Universitaria, Instituto de Ingeniería y Tecnología, Universidad Autónoma de Ciudad Juárez (UACJ), Ciudad Juárez, Chihuahua 32310, Mexico

Note: This paper was presented at the 67th Annual Conference on Magnetism and Magnetic Materials.
[a] **Authors to whom correspondence should be addressed:** maria.arreguin@ipicyt.edu.mx and jose.sanchez@ipicyt.edu.mx

ABSTRACT

Melt-spun ribbons samples of the multicomponent alloy $Mn_{0.5}Fe_{0.5}NiSi_{0.940}Al_{0.060}$ were prepared and the magnetostructural transition (MST) and related magnetocaloric properties studied for as-solidified ribbons and ribbon samples annealed between 800 and 950 °C for 4 h. The results are compared with those reported in the literature for melt-spun ribbons with an Al content x = 0.055 and bulk alloys. It is shown that all samples undergo a first-order MST from a paramagnetic Ni_2In-type hexagonal structure to a ferromagnetic TiNiSi-type orthorhombic one. Ribbons show broader isothermal entropy change $\Delta S_T(T)$ curves with moderate maximum values of $|\Delta S_T|^{max}$ at 2 T (7.2–7.3 J kg^{-1} K^{-1}) in comparison with the reported for bulk alloys. However, the average value of the magnetic hysteresis loss linked to the hexagonal-to-orthorhombic transition is low in comparison with the one reported for most magnetocaloric materials with first-order magnetostructural transitions. This work underlines the effectiveness of this rapid solidification technique to produce highly homogeneous ribbon samples of multicomponent alloys.

By substituting Si for Al in the ferromagnetic alloy $Mn_{0.5}Fe_{0.5}NiSi$ which derives from the MnNiSi system,[1] *Zhang et al.* reported the occurrence of magnetostructural transition (MST) in bulk $Mn_{0.5}Fe_{0.5}NiSi_{1-x}Al_x$ alloys.[2] In subsequent work,[3] theoretical calculations based on the density-functional-theory performed on the same alloy system demonstrated the existence of a giant magnetocaloric (MC) effect in $Mn_{0.5}Fe_{0.5}NiSi_{1-x}Al_x$ alloys with $0.045 \leq x \leq 0.070$; the experiments confirmed these results. These alloys show the highest peak value of the isothermal entropy change $|\Delta S_T|^{max}$ around room temperature for a magnetic field change ($\mu_0\Delta H$) of 2 T ever reported for a material undergoing a first-order magnetic phase transition. These results were later confirmed by further experimental work.[4–7] In these alloys, the MST on heating, which occurs from a ferromagnetic orthorhombic TiNiSi-type phase to a paramagnetic Ni_2In-type hexagonal one,[2,3] is highly sensitive to the Al content changing in a wide temperature range from 200 to 320 K when x decreases from 0.07 to 0.050.[2] In addition to the giant MC effect, it has been shown that the MST progressively shifts to a lower temperature with the increasing of the applied external pressure which predicts a large barocaloric

effect.[3] Due to the multi-elemental nature of these alloys, they are prepared by arc melting followed by prolonged thermal annealing at temperatures in the temperature range of 800–900 °C (typically several days)[4–7] But this does not avoid the presence of small amounts of spurious Mn-Al or "unidentified" secondary phases as detected in the reported X-ray diffraction (XRD) patterns by several authors.[2,3,5,8,9] In previous work, we explored the synthesis of the alloy $Mn_{0.5}Fe_{0.5}NiSi_{0.945}Al_{0.055}$ by rapid solidification using the melt spinning technique.[10] It was shown that the annealing time needed to produce the MST can be shortened to 4 h; moreover, the annealing temperature does not significantly change the structural temperature transition demonstrating this method's advantage in producing these alloys. Here, we report the magnetostructural and magnetocaloric behavior of $Mn_{0.5}Fe_{0.5}NiSi_{0.940}Al_{0.060}$ melt-spun ribbons making emphasis on the differences with respect to what has previously been observed for ribbon samples with Al content $x = 0.055$. It is shown that as-solidified ribbon samples already exhibit MST. When the annealing temperature is increased from 800 °C to 950 °C, the MST shifts to a higher temperature without a significant change in $|\Delta S_T|^{max}$ and the magnetic hysteresis loss.

A bulk ingot of the above-mentioned nominal composition was prepared by arc melting from highly pure Alfa Aesar elements: Mn 99.9998%, Fe 99.98%, Ni 99.99%, Si 99.9999%, and Al 99.999%. It was melted four times to ensure a good starting homogeneity to be liquefied by induction melting and ejected onto the polished surface of a 20 cm diameter copper wheel rotating at a linear speed of 10 ms^{-1}. Both processes were carried out under UHP Ar atmosphere in a MAM-1 arc melting furnace and a model SC melt spinner system from Edmund Bühler GmbH. To be thermally annealed, as-solidified (AS) ribbons flakes were sealed into vacuumed quartz ampoules; thermal annealing was interrupted by a fast quenching in iced water. Cu-K_α X-ray diffraction patterns were recorded on powdered samples in a Rigaku Smartlab high-resolution powder diffractometer. The microstructure and elemental chemical composition of the ribbon samples were examined by using a FEI SEM-QUANTA-250 scanning electron microscope (SEM) equipped with an EDAX EDS system. Differential scanning calorimetry (DSC) analyses were done in a TA Instruments model Q200 DSC system at a temperature sweep rate of 10 K min^{-1}. Magnetization measurements were performed by vibrating sample magnetometry in a Dynacool PPMS system from Quantum Design. Thermomagnetic curves were recorded under static magnetic fields of 5 mT and 2 T by sweeping the temperature at 1.0 K min^{-1}.

The typical granular microstructure of AS ribbon flakes in both the contact (CS) and non-contact (NCS) surfaces is shown in Figs. 1(a) and 1(b), respectively. As the pictures show, a smaller average grain size appears in the CS due to the constraining imposed on the nucleation and crystalline grain growth by the faster heat extraction during solidification. No gray contrasts were observed in the images suggesting that no secondary minor phases coexist with the matrix. The element distribution was checked by EDS mapping. As Figs. 1(d)–1(h) show all elements seem to be evenly distributed in the sample [the image of the area analyzed for the presented dot maps is shown in (c)]. More than 30 EDS spectra were randomly taken on both ribbon surfaces and the cross section [a typical one is shown in (i)], and from them the averaged elemental chemical composition was determined in at. % as $Mn_{16.7}Fe_{17.5}Ni_{32.4}Si_{30.6}Al_{2.8}$ which,

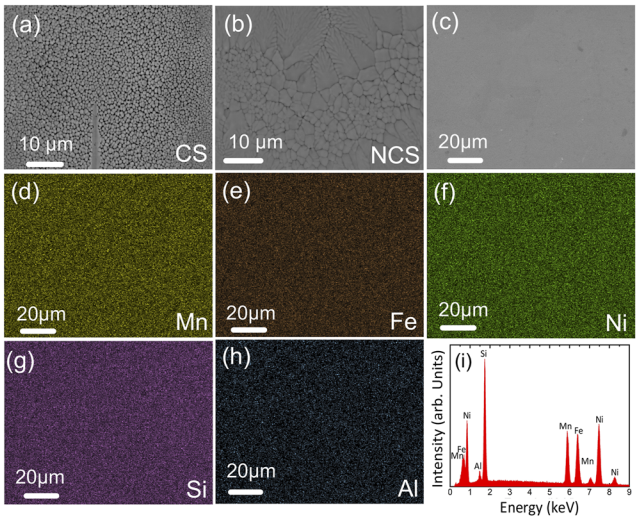

FIG. 1. As-solidified (AS) $Mn_{0.5}Fe_{0.5}NiSi_{0.940}Al_{0.060}$ ribbons: SEM images of both ribbon surfaces [CS (a) and NCS (b)], EDS element mapping images [from (c) to (h)] of Mn (d), Fe (e), Ni (f), Si (g) and Al (h), and typical EDS spectrum (i).

considering the error in the determination (~0.6 at. %), is not far from the nominal one (i.e., $Mn_{16.7}Fe_{16.7}Ni_{33.3}Si_{31.3}Al_{2.0}$).

The Le Bail fitting of the room temperature XRD patterns for AS and 850 °C annealed $Mn_{0.5}Fe_{0.5}NiSi_{0.940}Al_{0.060}$ ribbon samples are given in Figs. 2(a) and 2(b), respectively (whereas Fig. S1 shows the fitting for the samples annealed at 800 °C and 950 °C); the fitting was performed using the Fullprof suite package. In all of them, the Ni_2In-type is the major phase at room temperature coexisting with a minor amount of the TiNiSi-type one. The lattice constants and cell volume for both phases are listed in Table S1. The cell volume of the hexagonal phase remains almost unchanged, whereas that of

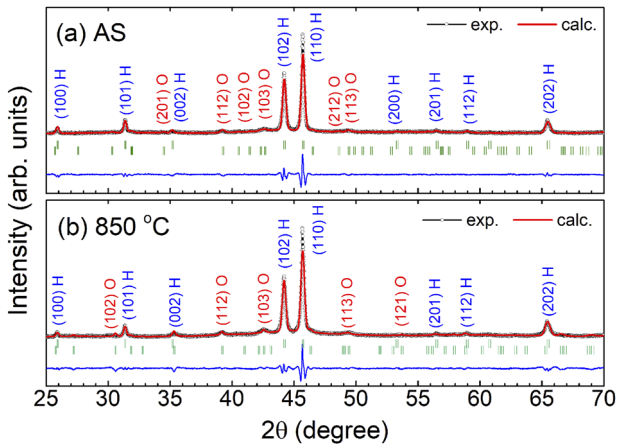

FIG. 2. Room temperature X-ray diffraction patterns for as-solidified (AS) (a) and 850 °C annealed (b) $Mn_{0.5}Fe_{0.5}NiSi_{0.940}Al_{0.060}$ ribbons; the vertical green bars indicate the Bragg positions of hexagonal and orthorhombic structures where as the difference between the experimental and calculated pattern is given by the bottom blue line.

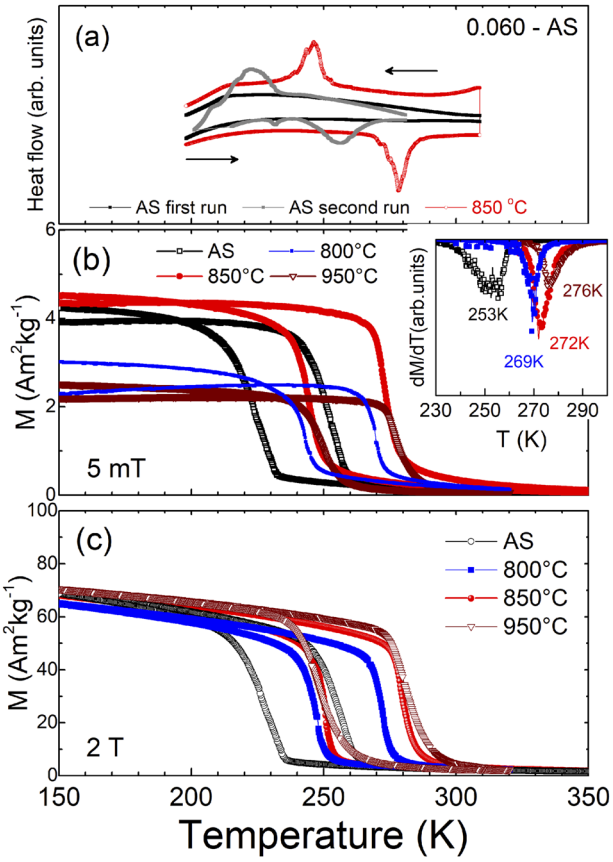

FIG. 3. DSC scans for AS ribbons (a), and $M(T)^{5mT}$ curves (b) with the respective $dM/dT(T)$ curves for the transition on heating at the inset, and $M(T)^{2T}$ curves (c) for AS and thermally annealed $Mn_{0.5}Fe_{0.5}NiSi_{0.940}Al_{0.060}$ ribbon samples.

the orthorhombic structure decreases as the annealing temperature increases.

Figure 3(a) shows the DSC scans for both AS and 850 °C annealed ribbon samples. As the graph shows, the AS sample does not exhibit structural transition after the first cooling to ~200 K (the lower T limit of our DSC instrument). So, to check the occurrence of the first structural transition from the hexagonal to the orthorhombic phase the sample was immersed in liquid nitrogen (i.e., to 77 K) and DSC runs were recorded. The figure shows that now broad exothermic and endothermic DSC peaks appear denoting the occurrence of the first-order transformation. The absence of the structural transition in the first DSC runs is due to the so-called "virgin effect" which derives from the large energy barrier that the strong internal stresses impose on the first structural transformation that on cooling appears at a much lower temperature. The stress release is manifested through the multiple cracking that mechanically deteriorates the alloy.[2,10] The *zero field-cooled* (ZFC) and *field-cooled* (FC) $M(T)$ curves at 5 mT displayed in Fig. 3(b) denote that AS and thermally annealed samples undergo a coupled MST being paramagnetic at RT. The inset in the figure shows the respective $dM/dT(T)$ curves for the heating transition (revealing a broader MST for AS samples), whereas Table I shows that the starting and finishing transition temperatures and thermal hysteresis ΔT_{hyst} determined by DSC and $M(T)^{5\,mT}$ are in good agreement (i.e., $\Delta T_{hyst} = A_f - M_S$). ΔT_{hyst} is large (around 30 K), but within the reported range for these alloys,[2,3,5–7] and tends to decrease when the annealing temperature increases. Interestingly, it is worth mentioning that AS ribbons show MST; Figs. S2(a) and S2(b) compare the $M(T)^{5\,mT}$ and $M(T)^{2\,T}$ curves for AS ribbons with $x = 0.060$ and 0.055. It is shown that the latter shows two successive broad transitions. If it is true that the transition for the AS samples appears at a lower temperature, Fig. 3(c) and Table I prove that, except for the 800 °C annealed ribbons, AS samples, and those annealed at 850 and 950 °C, exhibit almost the same magnetization change ΔM^{2T} at 2 T (43–47 $Am^2\,kg^{-1}$; estimated by simple extrapolation). Moreover, it is similar to the value reported for $x = 0.055$.[10] Increasing the annealing temperature, the MST temperature increases becoming nearly the same for 850 and 950 °C annealed samples. The observed changes in the MST temperature and saturation magnetization of the orthorhombic phase upon the annealing temperature provide insight into how the atomic rearrangement affects both parameters. If the thermomagnetic curves for $x = 0.060$ and 0.055 ribbon samples annealed at 850 °C are compared with those reported for bulk alloys,[3] the higher the Al content the lower the magneto-structural transition temperature.

TABLE I. Starting (A_S, M_S) and finishing (A_f, M_f) transition temperature, thermal hysteresis (ΔT_{hyst}), and magnetization change ($\Delta M^{2\,T}$) across the MST on heating for as-solidified (AS) and thermally annealed $Mn_{0.5}Fe_{0.5}NiSi_{0.940}Al_{0.060}$ ribbons samples.

Sample	Method	A_S (K)	A_f (K)	M_S (K)	M_f (K)	M_S (K)	ΔT_{hyst} (K)	$\Delta M^{2\,T}$ ($Am^2\,kg^{-1}$)
AS	DSC	242	268	234	212	234	34	44
	$M(T)^{5mT}$	245	260	234	213	234	26	
800 °C	DSC	263	276	243	227	243	33	31
	$M(T)^{5mT}$	262	272	234	224	234	38	
850 °C	DSC	272	286	252	239	252	34	43
	$M(T)^{5mT}$	270	280	251	239	251	29	
950 °C	DSC	269	281	250	233	250	31	47
	$M(T)^{5mT}$	274	283	255	242	255	28	

Figure 4(a) shows the $\Delta S_T(T)$ curves through the orth-to-hex MST (hereafter, the sample annealed at 800 °C has been excluded from the study) for $\mu_0\Delta H$ values from 0.5 to 2.0 T; for the sake of comparison, we included the curve previously obtained for 850 °C annealed ribbons with $x = 0.055$. All of them were obtained by numerical integration of the Maxwell relation from a set of isofield $M(T)$ curves measured always crossing the MST in the same direction (i.e., on heating; examples of the sets measured are shown in Fig. S3). The values of the main magnetocaloric parameters for the three ribbons samples characterized are given in Table II; this includes the refrigerant capacity (*RC*) values, which were estimated as follows:[11] (a) from the product $|\Delta S_T|^{max} \times \delta T_{FWHM}$ (*RC*-1), being δT_{FWHM} is the full-width at half-maximum of the $\Delta S_T(T)$ curve (i.e., $\delta T_{FWHM} = T_{hot} - T_{cold}$); (b) from the area under the $\Delta S_T(T)$ curve between T_{hot} and T_{cold} (*RC*-2);[12] and (c) maximizing the product $\Delta S_T \times \delta T$ below the ΔS_T curve (RC-3). As expected, the broader MST for AS samples leads to lower $|\Delta S_T|^{max}$. However, despite $\Delta S_T(T)$ curve peak appearing at a different temperature, the curves are similar in shape. Furthermore, the $|\Delta S_T|^{max}$ value measured does not change appreciably (7.2–7.3 J kg^{-1} K^{-1}) being nearly the same as the one previously found for $x = 0.055$ ribbon samples (7.8 J kg^{-1} K^{-1}). The broader MST shown by ribbons samples explains their inferior values of $|\Delta S_T|^{max}$ if compared with bulk alloys.[3,6] But, if the comparison is made based on *RC*, it is found that both ribbons and bulk exhibit similar values. Lastly, we also assessed the magnetic hysteresis loss *HL* in the temperature interval of the hex-to-orth MST for a maximum field of 2 T by measuring a set of isothermal magnetization curves applying and removing the magnetic field [as

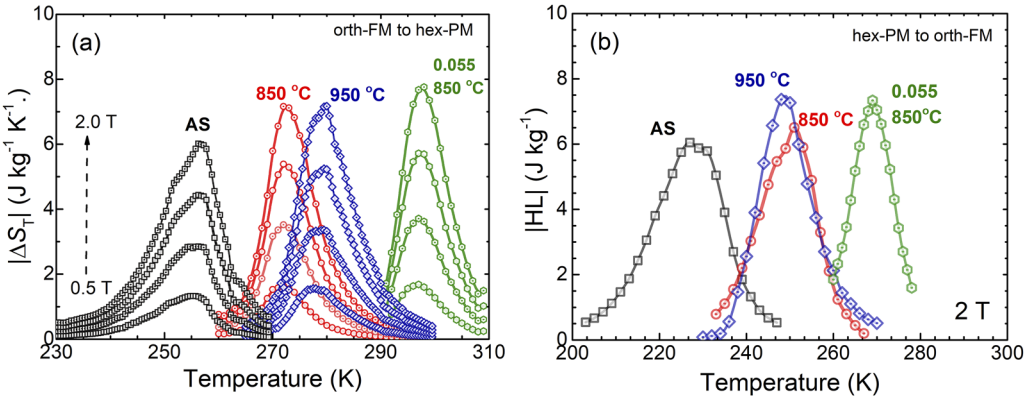

FIG. 4. $\Delta S_T(T)$ curves across the orth-to-hex MST for applied magnetic field changes from 0.5 to 2.0 T (a) and thermal dependencies of the magnetic hysteresis loss at 2 T for the hex-to-orth MST (b). For the sake of comparison, the curves corresponding to ribbon samples with $x = 0.55$ annealed at 850 °C are also represented.[10]

TABLE II. $|\Delta S_T|^{max}$, *RC*-1, *RC*-2, *RC*-3, δT_{FWHM}, and δT^{RC-3} through the orth-to-hex MST under magnetic field changes of 1 T and 2 T for AS and thermally annealed $Mn_{0.5}Fe_{0.5}NiSi_{0.940}Al_{0.060}$ ribbons. The data for ribbons samples with $x = 0.055$ thermally annealed at 850 °C is included for comparison purposes.[10] <*HL*> represents the average value of the magnetic hysteresis loss at 2 T over δT_{FWHM} for the hex-to-orth MST.

	0.060 AS		0.060–850 °C		0.060–950 °C		0.055–850 °C	
	$\mu_0\Delta H$ (T)		$\mu_0\Delta H$ (T)		$\mu_0\Delta H$ (T)		$\mu_0\Delta H$ (T)	
	1	2	1	2	1	2	1	2
$\|\Delta S_T\|^{max}$ (J kg^{-1} K^{-1})	2.9	6.0	3.5	7.2	3.4	7.3	3.7	7.8
<*HL*> (J kg^{-1})	···	5.0	···	5.1	···	5.2	···	6.0
RC-1 (J kg^{-1})	38	82	32	75	40	86	37	78
RC-2 (J kg^{-1})	30	64	28	60	32	67	30	64
T_{hot} (K)	260	262	277	278	285	286	303	303
T_{cold} (K)	247	248	267	268	273	274	293	293
δT_{FWHM} (K)	13	14	10	10	12	12	10	10
RC-3 (J kg^{-1})	19	41	18	39	20	44	19	40
δT^{RC-3} (K)	13	14	10	10	10	11	9	8
T_{hot}^{RC-3} (K)	260	262	278	278	284	285	302	302
T_{cold}^{RC-3} (K)	247	248	268	268	274	274	293	294

previously shown,[10] $M(\mu_0 H)$ curves upon increasing and decreasing the field across the orth-to-hex MST are reversible. Due to the large thermal hysteresis a large maximum magnetic field is needed to promote the transition]. To measure the $M(\mu_0 H)$ at each temperature, a *back-and-forward* thermal protocol was followed;[10] examples of the curves measured are given in Fig. S4. Figure 4(b) shows the thermal dependence of the magnetic hysteresis loss $HL(T)$. Its average value $<HL>$ over the δT_{FWHM} remains unchanged for the series, as was previously found for the $x = 0.055$. Indeed, if compared to other giant MC alloys such as Fe-Rh and (Ni, Mn)-based Heusler alloys it is very low (~5.0–6.0 J kg^{-1}).

To summarize: (a) the study carried out highlights the effectiveness of the rapid solidification method employed to synthesize highly homogeneous samples of these multicomponent $Mn_{0.5}Fe_{0.5}NiSi_{1-x}Al_x$ alloys; (b) no other phases than the hexagonal and orthorhombic were detected in the XRD patterns; (c) as solidified ribbons samples with $x = 0.060$ exhibits a well-defined magnetostructural transition, that shifts to a higher temperature as the annealing temperature increases; (d) in spite of the temperature at which that transition is tuned, both the shape and $|\Delta S_T|^{max}$ value of the entropy change curves remained almost unchanged.

See supplementary material for additional information about XRD and magnetization data of the studied samples.

Work supported by SEP-CONACyT, Mexico, under award A1-S-37066, Laboratorio Nacional de Nanociencias y Nanotecnologia (LINAN, IPICyT), and Slovak Grant Agency (VEGA 1/0404/21). The technical support received from LINAN's personnel M.Sc. B.A. Rivera-Escoto, M. Sc. A.I. Peña-Maldonado, and Dr. I.G. Becerril-Juárez is gratefully acknowledged. M.L. Arreguín-Hernández is grateful to The National Scholarship Programme of the Slovak Republic for the scholarship granted, and the CONACyT for supporting her Ph.D. studies (fellowship No. 861512). J.L. Sánchez Llamazares acknowledges the support received from the NextGenerationEU, MIU, and Plan de Recuperación, Transformación y Resiliencia, in the framework of the Maria Zambrano program of the University of Oviedo, Asturias, Spain (Reference: MU-21-UP2021-030 71741542).

AUTHOR DECLARATIONS

Conflict of Interest

The authors have no conflicts to disclose.

Author Contributions

M. L. Arreguín-Hernández: Data curation (equal); Formal analysis (equal); Funding acquisition (equal); Investigation (equal); Methodology (equal); Writing – original draft (equal); Writing – review & editing (equal). **A. Dzubinska**: Funding acquisition (equal); Software (equal). **M. Reiffers**: Funding acquisition (equal); Resources (equal). **J. L. Sánchez Llamazares**: Conceptualization (equal); Investigation (equal); Project administration (equal); Resources (equal); Supervision (equal); Validation (equal); Visualization (equal); Writing – review & editing (equal). **C. F. Sánchez-Valdés**: Data curation (equal); Funding acquisition (equal); Investigation (equal); Methodology (equal); Project administration (equal); Software (equal); Supervision (equal); Validation (equal). **R. Varga**: Project administration (equal); Resources (equal); Supervision (equal).

DATA AVAILABILITY

The data that support the findings of this study are available within this article and its supplementary material.

REFERENCES

[1] C. L. Zhang, H. F. Shi, Z. D. Han, B. Qian, C. Zhu, J. Chen, T. Z. Wang, and D. H. Wang, "The TiNiSi-to-Ni_2In-type magnetostructural transitions in alloys with largely reduced Ge-concentrations," Solid State Commun. **190**, 1 (2014).
[2] C. L. Zhang, H. F. Shi, Y. G. Nie, E. J. Ye, Z. D. Han, and D. H. Wang, "Thermal-cycling-dependent magnetostructural transitions in a Ge-free system $Mn_{0.5}Fe_{0.5}Ni(Si,Al)$," Appl. Phys. Lett. **105**, 242403 (2014).
[3] A. Biswas, A. K. Pathak, N. A. Zarkevich, X. Liu, Y. Mudryk, V. Balema, D. D. Johnson, and V. K. Pecharsky, "Designed materials with the giant megnetocaloric effect near room temperature," Acta Materialia **180**, 341 (2019).
[4] S. Ghosh, P. Sen, and K. Mandal, "Magnetostructural transition and large magnetocaloric effect in $(Mn_{0.6}Fe_{0.4})NiSi_{1-x}Al_x$ (x = 0.06–0.08) alloys," J. Magn. Magn. Mater. **500**, 166345 (2020).
[5] L. Lei, Z. G. Zheng, S. Jin, W. H. Wang, C. F. Li, J. Y. Liu, Z. G. Qiu, and D. C. Zeng, "The magnetostructural transition and magnetocaloric properties in $Fe_{0.6}Mn_{0.4}NiSi_{1-x}Al_x$ alloys," J. Appl. Phys. **128**, 013904 (2020).
[6] Taubel, "Designing multicaloric materials with martensitic phase transitions for future cooling applications," Ph.D. thesis, Technische Universität, Darmstadt, Germany, 2021.
[7] M. Khan, R. C. Das, J. Casey, B. L. Reese, B. Akintunde, and A. K. Pathak, "Near room temperature magnetocaloric properties in Ni deficient $(Mn_{0.252}Fe_{0.5})Ni_{0.975}Si_{0.95}Al_{0.05}$" AIP Adv. **12**, 035227 (2022).
[8] A. Biswas, N. A. Zarkevich, Y. Mudryk, A. K. Pathak, A. V. Smirnov, V. P. Balema, D. D. Johnson, and V. K. Pecharsky, "Controlling magnetostructural transition and magnetocaloric affect in multi-component transition-metal-based materials," J. Appl. Phys. **129**, 193901 (2021).
[9] B. Nuendute, W. Hanggai, H. Yibole, B. Tana, O. Tegus, and F. Guillou, "Drastic influence of synthesis conditions on structural, magnetic, and magnetocaloric properties of Mn(Fe,Ni)(Si,Al) compounds," Crystals **12**, 233 (2022).
[10] M. L. Arreguín-Hernández, C. F. Sánchez-Valdés, and J. L. Sánchez Llamazares, "Magnetostructural transition and magnetocaloric effect in thermally annealed $Mn_{0.5}Fe_{0.5}NiSi_{0.945}Al_{0.055}$ melt-spun ribbons," J. Magn. Magn. Mater. **533**, 168021 (2021).
[11] P. Gorria, J. L. Sánchez Llamazares, P. Álvarez, M. J. Pérez, J. Sánchez Marcos, and J. A. Blanco, "Relative cooling power enhancement in magneto-caloric nanostructured Pr_2Fe_{17}," J. Phys. D: Appl. Phys. **41**, 192003 (2008).
[12] A. Quintana-Nedelcos, J. L. Sánchez Llamazares, C. F. Sánchez-Valdés, P. Álvarez Alonso, P. Gorria, P. Shamba, and N. A. Morley, "On the correct estimation of the magnetic entropy change across the magneto-structural transition from the Maxwell relation: Study of $MnCoGeB_x$ alloy ribbons," J. Alloys Compd. **694**, 1189 (2017).